Supplementary Information

Table S1: Sub-event model of the 2013 Okhotsk earthquake

	Times (s)	Longitude (°)	Latitude (°)	M_w
I1	1.33	153.278	54.877	7.10
E1	8.94	153.347	54.898	7.95
E2	15.30	153.507	54.475	8.13
E3	22.95	153.471	54.823	7.88
E4	24.23	153.653	54.160	7.95
E4	32.27	153.656	54.135	7.42

Table S2: Sub-event model of the 1994 Bolivia earthquake

	Times (s)	Longitude (°)	Latitude (°)	M_w
E1	0.04	-67.561	-13.845	7.18
E2	3.34	-67.425	-13.880	7.14
E3	6.55	-67.416	-13.849	7.24
E4	11.77	-67.227	-13.884	7.71
E5	15.96	-67.208	-13.840	7.81
E6	20.67	-67.406	-13.729	7.71
E7	26.11	-67.322	-13.697	7.91
E8	35.04	-67.241	-13.764	7.51
E9	32.55	-67.003	-13.682	7.61

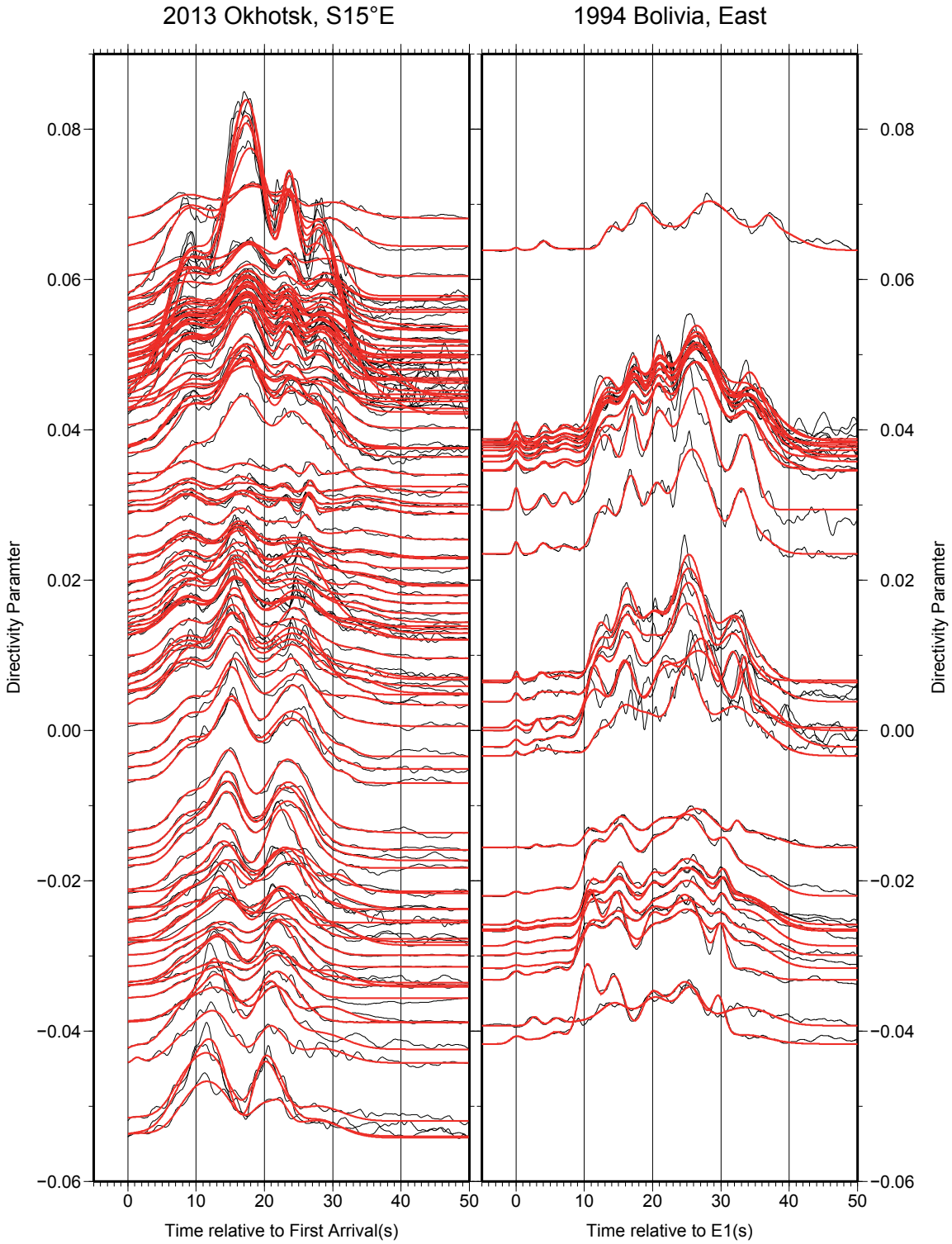

Fig. S1: Waveform fits for the sub-event models of the 2013 Okhotsk earthquake and 1994 Bolivia earthquake. The data is plotted in black and the synthetics are plotted in red.

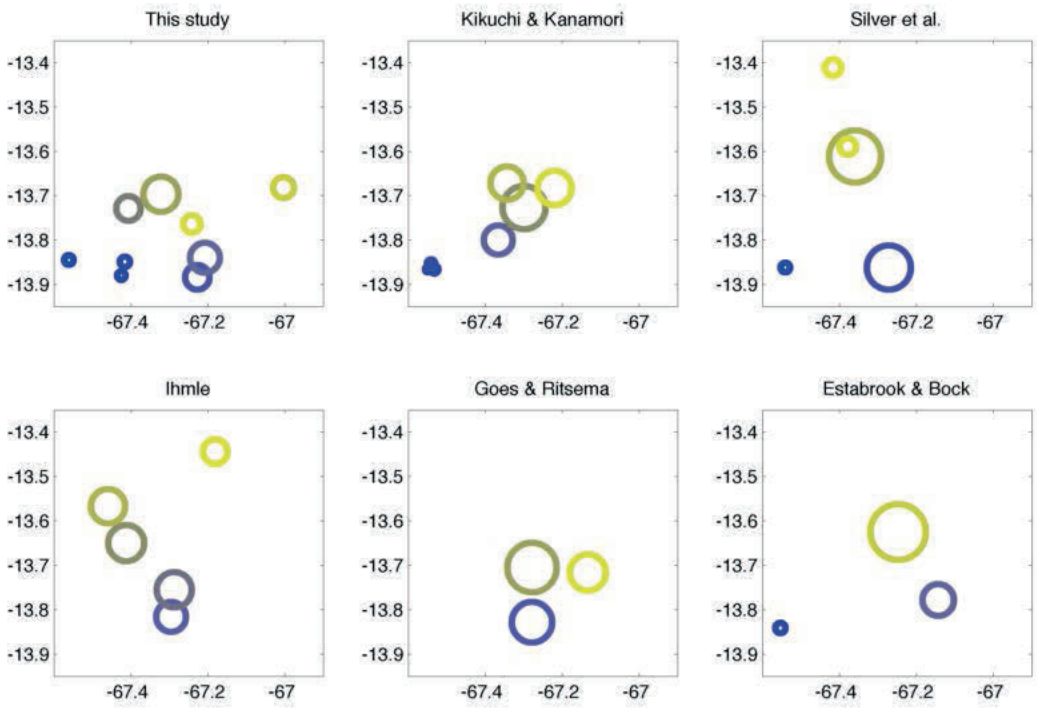

Fig. S2: Comparison of the sub-event models obtained in this study and previous studies by Kikuchi & Kanamori (1994), Silver et al. (1995), Ihmle (1998), Goes & Ritsema (1995), and Estabrook & Bock (1995)[3-7]. The sizes of the circles are proportional to sub-event moments, and the colors indicate sub-event centroid times (from blue at 0s to yellow at 40s). The overall rupture dimensions from different studies are consistent, with all of them being roughly ~30km×40km. The approximately eastward rupture in stage 1 is resolved by Kikuchi & Kanamori, Silver et al., and Estabrook & Bock, although none of the other studies separately resolve the locations of the 3 early, smaller sub-events of our model (E1, E2, E3). The rupture directions in stage 2 are toward the north, northwest or northeast, also consistent with our sub-event model.

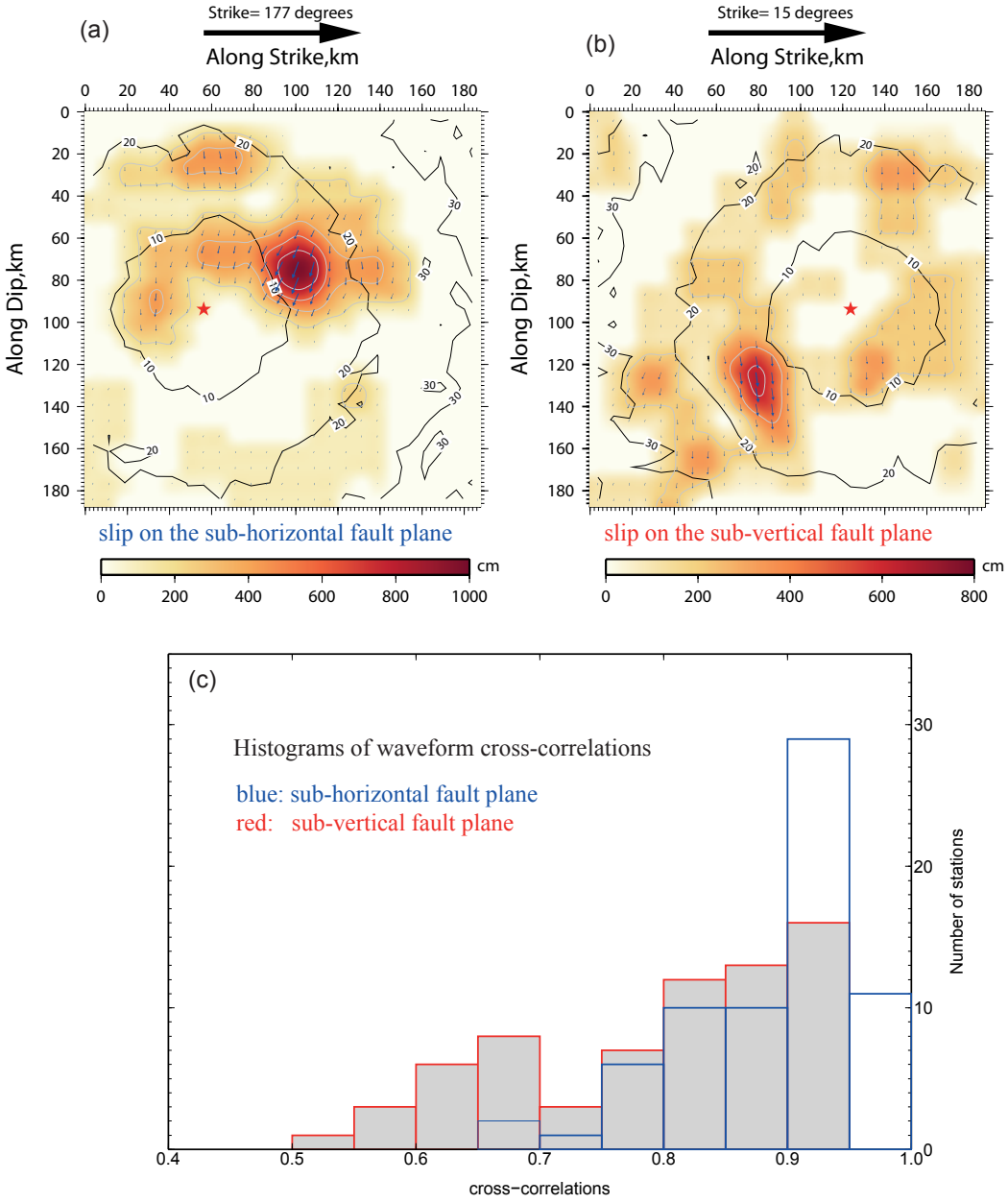

Fig. S3: (a) and (b) show finite-fault inversions assuming the near-horizontal or near-vertical fault planes of the NEIC W-phase moment tensor, respectively. The near-horizontal fault plane has a strike of 177° and dip of 10° whereas the conjugate fault plane has a strike of 15° and dip of 80°, and rupture is only allowed on a single fault plane in these finite-fault inversions. We use 69 teleseismic P-wave velocity waveforms with good azimuthal coverage and a simulated annealing inversion scheme to simultaneously invert for rake, slip amplitude, average rupture speed and rise time on each subfault[8]. During the inversions we allow the slip to vary from 0 to 20m in intervals of 1m, and the rupture speed can vary from 3.5 to 4.5 km/s, in intervals of 0.1 km/s. Rupture back towards the hypocenter is not allowed, and therefore the slip pattern cannot reproduce the slip distribution preferred by our sub-event analysis. The background color denotes slip amplitude and the rupture times are shown as contours. (c) Histograms of cross-correlations between synthetics and data for both finite-fault models, with the near-horizontal fault plane in blue and sub-vertical fault plane in red. The model with the near-horizontal fault plane has significantly better data fits compared with the model with the near-vertical fault plane (mean cross-correlation of 0.89 versus 0.80). This difference in cross-correlations is further supported by waveform comparisons for both models in Fig. S6 and Fig. S7, respectively.

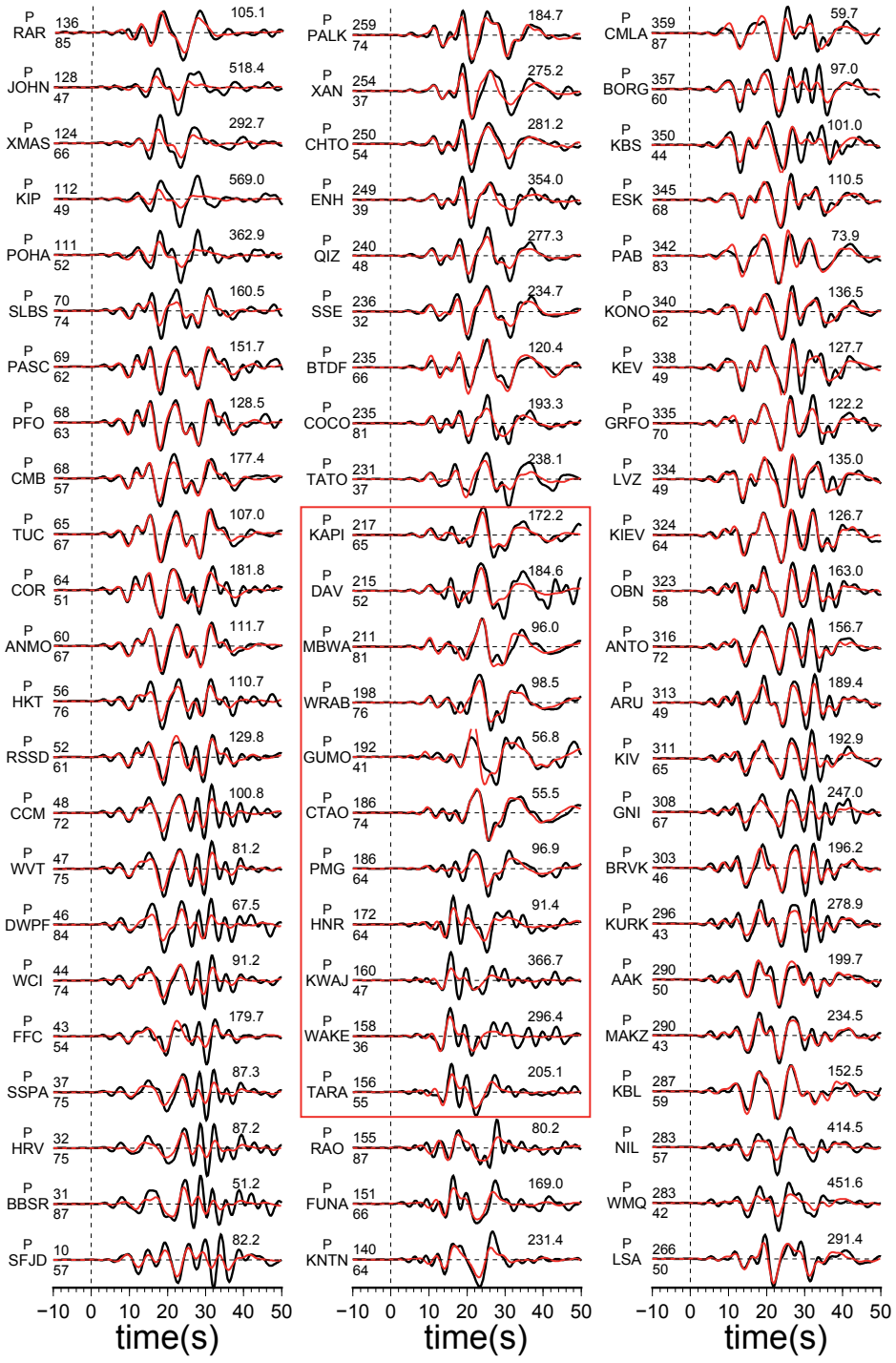

Fig. S4: Waveform fits for the finite-fault inversion with the sub-horizontal fault plane. For each station, the station names are displayed to the left, followed by the station azimuth (upper number) and distance (lower number) in degrees. The number near the end of each trace is the amplitude in μm/s. Both data (black) and synthetics (red) are filtered to periods longer than 3 s. The red box highlights stations with significant differences in waveform fits in Fig. S6 compared with those of Fig. S7.

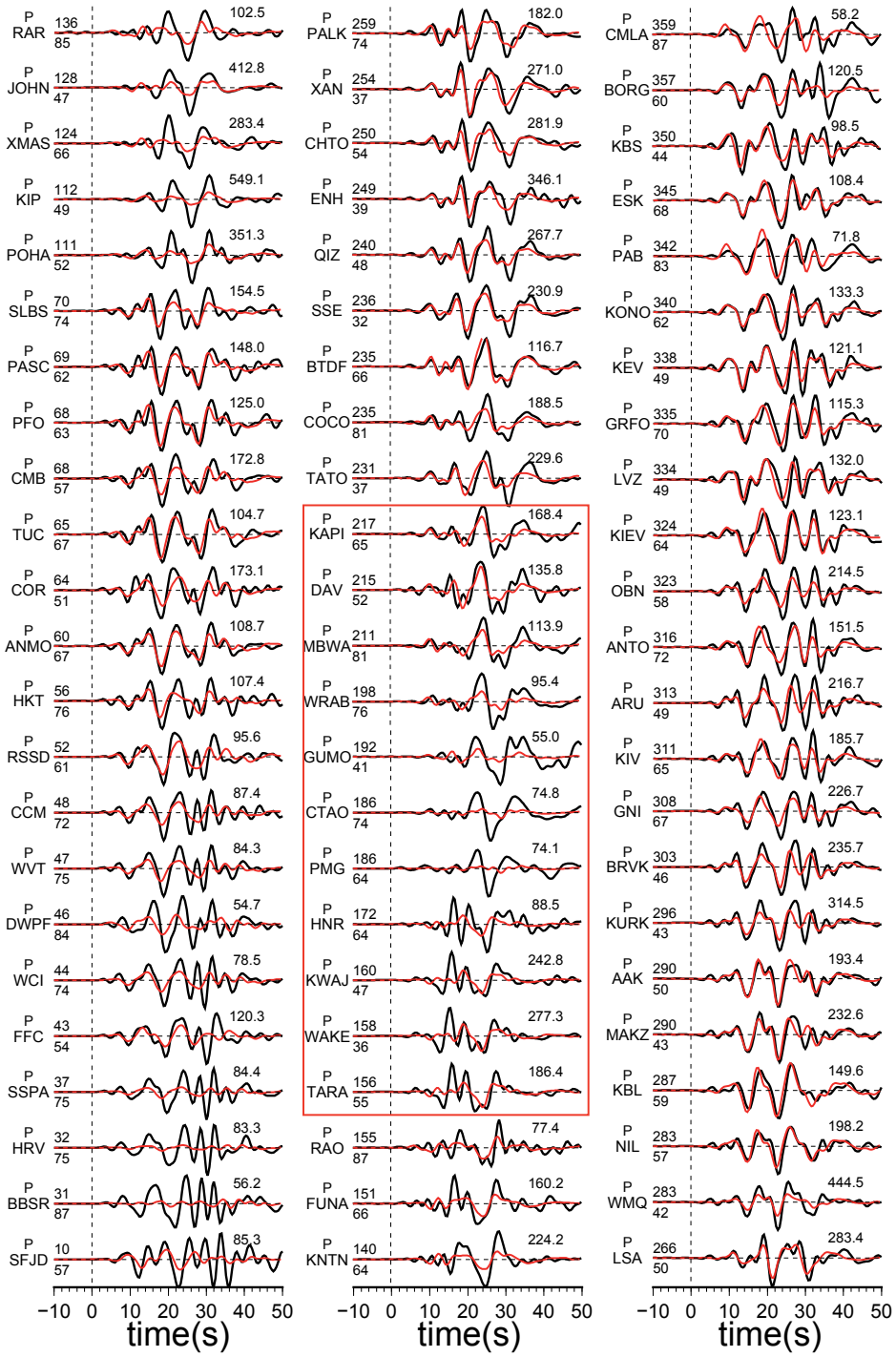

Fig. S5: Waveform fits for the finite-fault inversion with the sub-vertical fault plane. Labels are as in Fig. S6.

References

1 Kikuchi, M. & Kanamori, H. The mechanism of the deep Bolivia earthquake of June 9, 1994. Geophysical Research Letters 21, 2341-2344 (1994).

2 Silver, P. G. et al. Rupture characteristics of the deep Bolivian earthquake of 9 June 1994 and the mechanism of deep-focus earthquakes. Science 268, 69-69 (1995).

3 Goes, S. & Ritsema, J. A broadband P wave analysis of the large deep Fiji Island and Bolivia earthquakes of 1994. Geophysical research letters 22, 2249-2252 (1995).

4 Estabrook, C. H. & Bock, G. Rupture history of the Great Bolivian Earthquake: Slab interaction with the 660-km discontinuity? Geophysical Research Letters 22, 2277-2280 (1995).

5 Ihmlé, P. F. On the interpretation of subevents in teleseismic waveforms: the 1994 Bolivia deep earthquake revisited. Journal of Geophysical Research 103, 17919-17932 (1998).

6 Ji, C., Wald, D. J. & Helmberger, D. V. Source description of the 1999 Hector Mine, California, earthquake, part I: Wavelet domain inversion theory and resolution analysis, Bull. Seismol. Soc. Am., 92(4), 1192-1207 (2002).